Stirring and Mixing by Vortical Modes

Jennifer MacKinnon

Abstract

Tracer release experiments in coastal and open ocean settings have revealed unexpectedly large isopycnal diffusivities. The stirring and mixing effects of small scale eddies (vortical modes) are discussed as a possible candidate for enhancing diffusivity. A simple analytical model of vortical modes is used to evaluate their mixing potential.

1 Introduction

Recent oceanic dye release experiments have provided a venue for evaluating existing models of passive tracer horizontal dispersion. In the Coastal Mixing and Optics (CMO) experiment and the North Atlantic Tracer Release Experiment (NATRE), anthropogenic dye was injected along constant density surfaces (isopycnals) in streaks a few km long. Subsequent surveys through the evolving dye patches with towed instruments were used to look at the qualitative nature of dye patch evolution and calculate quantitative measures of isopycnal diffusion [1, 2].

In the CMO experiment, several mid-water-column dye releases were conducted between 1995 and 1997 in $\sim$ 80 m deep water on the continental shelf south of New England. Post release surveys were conducted over the several days following each release. By assuming that dye streak evolution was governed by a balance between horizontal diffusion and strain induced stretching [3], Sundermeyer 98 calculates an observed horizontal diffusivity of .3-5 m^2/s [1]. A traditional way of estimating horizontal diffusivity in the ocean is by looking at the enhanced diffusivity that comes from combining vertical diffusion with shear from the internal wave field [4]. Applying this method to the measured CMO velocities gives diffusion estimates that are a factor of 1-10 below observed values[1].

The NATRE experiment was conducted in open ocean 1200 km west of the Canary Islands during May 1992 [2]. The dye was sampled five times during several subsequent years. Over this extended period, the qualitative evolution of the dye agrees reasonably well with the model of horizontal diffusion presented by Garrett 83 [1]. He proposes that a dye patch will initially be stretched into long twisted streaks, the width of which is governed by a balance between an effective isopycnal diffusivity and exponential stretching. The observed dye at 6 months is indeed streaky in nature and calculations give an estimated effective diffusivity of 3 m^2/s. The Young, Rhines and Garrett shear dispersion model applied to this situation gives an estimate of .08 m^2/s [1]. For longer times, Garrett predicts that dye streaks will coalesce into a more homogeneous patch that grows with an effective diffusivity related to the Lagrangian velocity autocorrelation time scale. During later dye surveys (1-2 years), the tracer has expanded to encompass hundreds of kilometers and is more homogeneous. The observed diffusivity for this scale is 10^3 m^2/s, and agrees with estimates calculated from float velocities.

In both experiments, observed diffusivities on 1-10 km scales are larger than predicted by shear dispersion alone. Both Sundermeyer and Polzin et al.99 propose that the small scale eddies known as vortical modes could be an alternate diffusion mechanism. In brief, vortical modes are thought to be generated when a vertical mixing event creates a relatively well mixed patch of water within a stratified fluid [5]. This density anomaly adjusts to pressure and Coriolis forces by spreading radially outward and beginning to rotate anticyclonically. A steady rotational state can exist until the anomaly diffuses away or some event or instability breaks it apart. Both the adjustment and equilibrium phases can act to enhance horizontal diffusivity.

Sundermeyer considers dimensional arguments and concludes that in the coastal ocean at least, horizontal spreading from vortical mode generation and adjustment may be of an appropriate magnitude to explain observed diffusivities [1]. Polzin et al. evaluate evidence of vortical modes in NATRE by looking at spectral shear and strain values that are not well explained by an internal wave field. Using inferred vortical mode spectra, they calculate estimates for shear dispersion and stirring contributions to effective diffusivity and also get results potentially large enough to explain observations[6].

To tackle the time dependent picture of diffusivity due to vortical modes, we start with a broad qualitative description of what might happen to an initially small dye patch in an ocean where small eddies randomly appear and disappear in various locations near the patch. We ignore the initial vertical mixing event that generates the vortical mode as beyond the scope of this project. Instead we assume that we start with a round (axisymmetric) density anomaly that abruptly appears near a small patch of concentrate. Over the lifetime of a single vortex, a small dye patch located nearby feels a net (center of mass) displacement both outward due to the initial adjustment and around the vortex. The patch also feels a distortion due to the stretching effects of radial shear and molecular and shear-enhanced diffusion. On a longer timescale, the patch will witness the appearance and disappearance of many vortices appearing at different positions around it. Additionally, as it grows in size it eventually becomes large enough to feel several spatially separated vortices at the same time. The larger the number of vortices felt, the more their net displacements will cancel out to produce little net patch movement. However, the net movements felt by smaller segments of the patch stretch, twist, and fold the patch; increase gradients; and enhance diffusion to cause the patch as a whole to grow in size. We seek an understanding of diffusion that will encompass both small and large time limits. For small times, we'll have a more time dependent story of patch growth. For larger times and larger spatial scales we hope that the net effects of smaller motions can be parameterized by an effective diffusivity. Our goals hence are threefold: to understand the time dependence of small time evolution, to estimate a long time eddy diffusivity, and to figure out an appropriate time scale for transition between these two regimes.

Toward these goals, we develop a a simple analytical model that we hope replicates some of the essential stirring and mixing characteristics of oceanic vortical modes. Such an analytical approximation allows us to look at the role small eddies may play in the different stages of horizontal tracer dispersion, get some bounds on the relative importance of different diffusive mechanisms, and explore how these results are functions of fundamental problem parameters. In section 2 we begin by looking at numerically integrated full numerical solutions for vortical mode generation. Based upon these solutions, in Section 3 we suggest an analytical approximation for a vortical mode field and extend it into a time dependent stochastic model. In section 4 we evaluate the expected effect of an idealized single vortex velocity field on the evolution of a dye patch. We expand the time scale to consider a time dependent blinking vortex field in section 5. Throughout, we try to integrate different ways of looking at diffusion and consider dependence on a few oceanographic parameters of interest. Finally, in section 6 we re-dimensionalize our results and make some simple comparisons to the observed ocean values.

2 Vortical Mode Solutions

Before we can develop an appropriate analytical model, we must first get a better feeling for physically realistic vortex velocity fields. We start with the generation of the density anomalies that become vortical modes. We then numerically solve for the equilibrium solutions that describe the velocity field after an adjustment period. Finally, we consider physical arguments for time dependence.

2.1 Generation Possibilities

Many observations have shown diapycnal mixing in the ocean to occur episodically [7]. Energetic events such as internal wave breaking and wave wave interaction can lead to shear instabilities and overturning. Such mixing events produce local regions of relatively unstratified water. Most observations of mixed patch height in the CMO coastal area range from 2-10 m [1]. In the NATRE experiment, observed vertical patch sizes were much larger, on the order of 10-50 m [6]. It is difficult to measure the horizontal extent of mixing events. A starting guess is that the mixed patches have roughly the same aspect ratio as the internal waves that generate them, N/f (where N is the buoyancy frequency and f the local inertial frequency). Microstructure sections made during the CMO experiment show mixing patches on the order of a kilometer in horizontal extent [8].

Following Garrett and Munk, we estimate the frequency of vertical mixing events by considering net observed vertical diffusivity[1]. We assume that vertical diffusion of tracer is due to the sum of discrete identical vertical mixing events which occur with a frequency ν, are characterized by height h_*, and by stratification change ΔN^2. Using potential energy arguments we can infer the frequency of event occurrence given an observed vertical diffusivity of K_z,

$$\nu = 3\frac{N^2}{\Delta N^2}\frac{1}{h^2}K_z. \tag{1}$$

2.2 Adjustment

A density anomaly of sufficient size in a stratified fluid will evolve according to the pressure and Coriolis forces it feels until a state of balance is achieved. In studying the equilibrium solution reached after adjustment of an initial density anomaly, we follow McWilliams tactic of combining the thermal wind equations with conservation of potential vorticity and mass [9]. He starts by non-dimensionalizing as follows:

$$
\begin{aligned}
q_d &= f N_*^2 q \\
\theta_d &= \frac{\rho_* v_* f l_*}{g h_*} \theta \\
r_d &= l_* r \\
z_d &= h_* z \\
p_d &= \rho_* v_* f l_* \\
\rho_d &= \frac{\rho_* N_*^2 h_*}{g} \rho \\
v_d &= v_* v,
\end{aligned}
$$

where the subscript 'd' indicates the dimensional form of a variable. Variables without this subscript (now and throughout this paper) are assumed to be dimensionless. Variable q is Ertel's potential vorticity, θ is the density anomaly (deviation from constant stratification) and the other variables have their traditional meaning (radial and vertical distance, pressure, density and velocity respectively). Important non-dimensional parameters are given by

$$
\begin{aligned}
R &\equiv \frac{4 v_*}{f l_*} \\
B &\equiv \left(\frac{N_* h_*}{f l_*}\right)^2 \\
\beta &\equiv \frac{R}{4B}.
\end{aligned}
$$

R and B are the Rossby and Burger numbers. β can be shown to be a measure of the strength of the density anomaly, with initial density and stratification profiles given non-dimensionally by

$$
\begin{aligned}
\rho_i &= -z + \beta\theta \\
N_i^2 &= 1 - \beta \frac{\delta\theta}{\delta z}.
\end{aligned}
$$

(We use β instead of McWilliams γ because the later is used as a stretching rate in later sections.) Following McWilliams, we assume an initial density anomaly of the form

$$\theta = 2z e^{-[z^2 + (r/r_0)^2]}. \tag{2}$$

At this point, parameters r_0 and B both describe an aspect ratio of the problem. Without loss of generality, we can set B=1 and vary r_0.

For simplicity, we adopt these non-dimensionalizations for the remainder of our paper. Physically, all horizontal distances, angular velocities and times discussed are fractions of the internal Rossby radius, intertial frequency and inertial period respectively. To convert any result back into dimensional coordinates, one only needs to specify f, N and an anomaly height scale h_*. Dimensional quantities are then given by

$$r_d = \frac{N}{f} h_* r \tag{3}$$

$$\Omega_d = f\beta\Omega \tag{4}$$

$$t_d = \frac{1}{f\beta} t. \tag{5}$$

We'll return briefly to the world of dimensions at the end of the paper to compare our results with oceanographic data.

The actual process of geostrophic adjustment will involve internal waves which radiate energy away in a time roughly given by $1/f$ [10]. After the transients have disappeared, the system will achieve an equilibrium state where Coriolis, pressure and centrifugal forces are in balance. Equilibrium density and potential vorticity are given by

$$\begin{aligned} \rho_f &= -z - \beta\frac{\partial p}{\partial z} \\ q_f &= ZN_s^2 - \frac{R\beta}{4S}\left(\frac{\delta^2 p}{\delta r \delta z}\right)^2 \end{aligned}$$

with

$$\begin{aligned} S &\equiv \sqrt{1 + \frac{R}{r}\frac{\partial p}{\partial r}} \\ v &\equiv \frac{2r}{R}[S-1] \\ Z &\equiv 1 + \frac{R}{4r}\frac{\partial (rv)}{\partial r}. \end{aligned}$$

Knowledge of one variable, $p(r, z)$, is enough to specify the whole system. This final state is related to the initial state through the net displacements felt by each Lagrangian water parcel. Non-dimensional displacement variables are defined as

$$\zeta(r_f, z_f) \equiv r_f - r_i \tag{6}$$

$$\eta(r_f, z_f) \equiv z_f - z_i. \tag{7}$$

These parcels conserve their density and potential vorticity values during adjustment

$$\rho_f(r, z) = \rho_i(r - \zeta, z - \eta) \tag{8}$$

$$q_f(r, z) = q_i(r - \zeta, z - \eta). \tag{9}$$

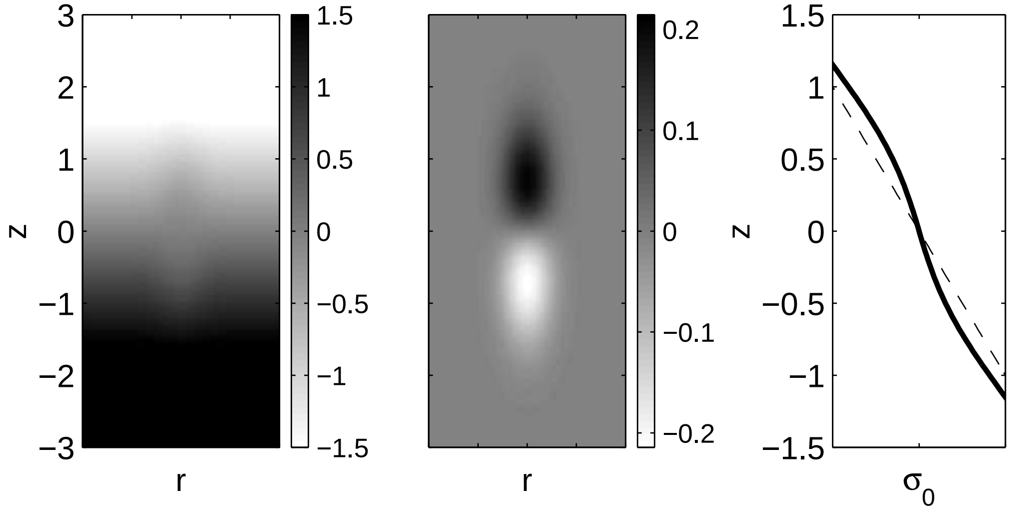

Figure 1: Pre-adjustment density field used for numerical calculations. The full density field is shown in (a), the density anomaly in (b), and a vertical profile at $r = 0$ in (c). Also shown in (c) is a reference linear stratification profile. All values are non-dimensional.

Plugging forms for ρ_i, ρ_f, q_i, q_f into equations (8) and (9) gives us two equations and three unknowns (p,ζ,η). The final equation comes from requiring that the adjustment be incompressible, or equivalently that the Jacobian of the lagrangian transformation is identically one:

$$\frac{r_i}{r_f}\left(\frac{\delta r_i}{\delta r_f}\frac{\delta z_i}{\delta z_f} - \frac{\delta r_i}{\delta z_f}\frac{\delta z_i}{\delta r_f}\right) = 1, \tag{10}$$

where r_i, r_f, z_i, z_f can be written in terms of ζ and η following equations 6-7. As McWilliams suggests, an iterative method is necessary to solve the non-linear set of equations 8-10 for p,ζ,η. There are only two free parameters in this system, r_0 and β, which control the aspect ratio and strength of the initial anomaly, respectively. Physically, $r_0 = 1$ corresponds to an anomaly with aspect ratio f/N. Larger r_0 corresponds to a flatter anomaly and vice versa. The anomaly strength is controlled by β, which ranges from 0 (no anomaly, or background stratification) to .5 (minimum of zero stratification). Figure 1 shows an initial density field with $r_0 = 1$, $\beta = \frac{1}{4}$,the associated density anomaly, and a profile of density at $r = 0$ (with linear stratification for comparison). These values of r_0 and β will be used as a good first estimate.

We numerically integrated solutions to equations (8), (9), and (10) [1]. Boundary conditions

[1]Numerical integration was done using routines AVINT and HSTCYL, available from the NIST Guide to Available Math Software

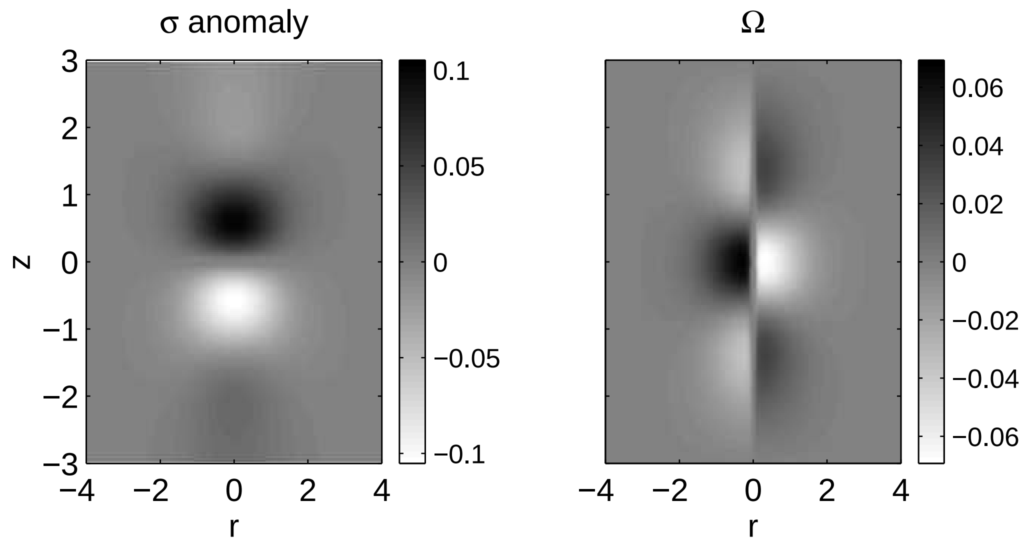

Figure 2: Equilibrium solutions for the density anomaly (a) and angular velocity (b).

are given by

$$\eta, \zeta, p \to 0 \qquad as \qquad r, z \to 0 \tag{11}$$

$$\zeta = \frac{\partial p}{\partial r} = 0 \qquad at \qquad r = 0 \tag{12}$$

$$\eta = \frac{\partial p}{\partial z} = 0 \qquad at \qquad z = 0. \tag{13}$$

$$\tag{14}$$

As expected, equilibrium solutions consist of a slumped density anomaly rotating anti-cyclonically. Figure 2 shows non-dimensional equilibrium density and angular velocity fields. Above and below the main anomaly, there are smaller, cyclonically rotating vortices that correspond to regions of enhanced stratification that border the well mixed patch. We ignore these smaller vortices for now and hope to come back to them in future work.

Figure 3 shows profiles at $z = 0$ of radial adjustment displacements, ζ, and equilibrium angular velocities. Adjustment displacements are largest at the edge of the initial anomaly ($r = r_0 = 1$), and have a maximum value that approaches 1 as r_0 becomes large. Angular velocity is roughly given by solid body rotation out to $r \sim .5$, and exponentially decays for larger r. Also shown is an analytical approximation of velocity that will be used in later sections. Further dependence on parameters r_0 and β is considered by McWilliams. The effect of varying these parameters on our diffusion calculations may be discussed in future work.

2.3 Time dependence

As isolated vortical mode will exist in its equilibrium state until the density anomaly diffuses away, another vertical mixing event occurs on top of it, or it succumbs to some type of

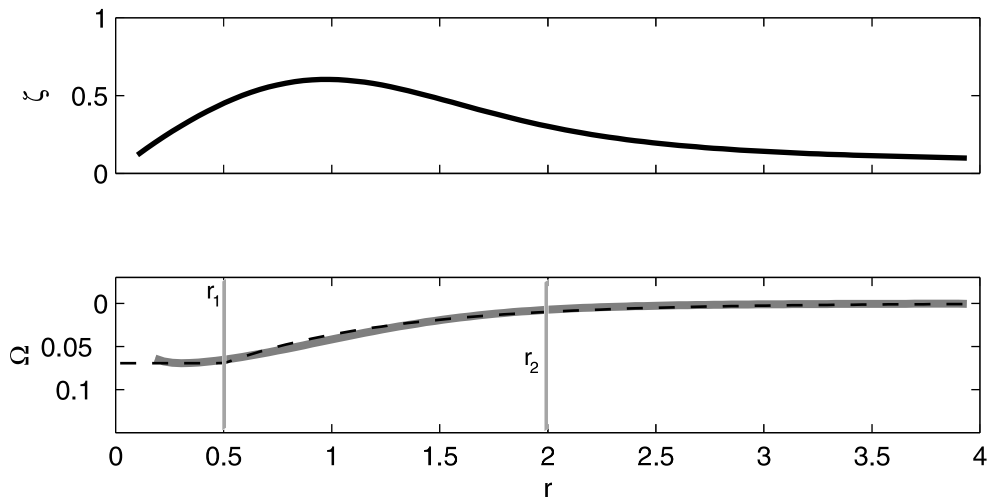

Figure 3: Outward adjustment displacements (a) and equilibrium radial velocity (b) at z=0 for $r_0 = 1$ and $\beta = .25$. Also shown are distances r_1 and r_2 which are the edge of solid body rotation and an effective edge of vortex influence.

instability or large scale strain. The time scale for vertically mixing an anomaly of height h away by a molecular vertical diffusivity K_{zm} is

$$\tau_1 = \frac{h^2}{K_{zm}}. \tag{15}$$

A new vortex will on average appear at a particular site with a frequency given by (1). Since molecular diffusivity will always be smaller than observed diffusivity, we expect the maximum lifetime for vortices will be given by

$$\tau \equiv 1/\nu.$$

For the coastal ocean observed patch size of 2-10 m and observed vertical diffusivity of $10^{-5} m^2/s$, the appropriate dimensional timescale is $\tau_d = 1 - 20$ days . In non-dimensional units, $\Omega\tau = .01 - .3$. In most cases, significantly less than one rotation is completed. In the open ocean, patch heights of $10-50$ m and diffusivities of $.5-1*10^{-5} m^2/s$ give nondimensional $\Omega\tau = .3 - 15$ (All calculations assume $\Omega = .07$.) In the later case vortices can exist in equilibrium form for many rotations. This difference in the time scale of vortical modes in different regions is in itself a major result. We expect that the ways in which vortical modes contribute to diffusion may be significantly different in these two situations. Hence, it will be a primary goal of subsequent calculations to consider how vortical mode enhanced diffusion both qualitatively and quantitatively depends on our choice of τ.

3 Analytical Model

We now wish to consider the diffusive effects of a field of such vortices. To make our task tractable, we incorporate an analytical approximation to the solutions in section 2 into a simple Random Renovating Vortex model that allows us to stochastically approach diffusion quantities of interest. We posit a field of vortices, each of which appears in a random location, exists for a set time τ, identical for all vortices, and disappears. Associated with the appearance of any vortex are instantaneous adjustment displacements ζ outward from the vortex center. During the subsequent interval τ of vortex existence, water parcels follow a steady azimuthal velocity field, $\Omega(r)$. For simplicity, we basically ignore z dependence from now on (except when considering vertical shear dispersion). We hope a first order picture of the dispersive abilities of vortical modes will emerge from considering the radial dependence alone. Future work may include a more baroclinic model. The numerical solutions to McWilliams equations suggest analytical forms as follows. Let the azimuthal velocity field a distance r from the center of the vortex be given by

$$\Omega(r) \equiv \begin{cases} \Omega_0 & r < r_1 \\ \Omega_0 e^{-\alpha(r-r_1)} & r \geq r_1. \end{cases} \tag{16}$$

The free parameters are r_1, the edge of the solid body rotation part of the vortex, Ω_0, the velocity scale, and α, the exponential decay rate for the outer vortex velocity field. Fitting this model to the numerical solution shown in Figure 3 yields $r_1 = .5$, $\alpha = 1.3$, and $\Omega_0 = .07$. Also noted on the graph is a distance r_2, which we define as a length-scale of vortex influence. It should scale roughly with the exponential decay scale, $r_2 \sim 1 + 1/\alpha$. For simplicity, we set $r_2 = 2$.

Simplifying further, we assume a parcel at any given location feels only one vortex at a time and that vortices do not interact with each other. Despite these caveats, we want vortices to be evenly distributed in space, in some statistical sense. Hence, we propose that the probability of a vortex appearing within r and $r + dr$ of a given parcel is given by the Holtzmark distribution,

$$P(r) \equiv \frac{2}{r_2^2} r e^{-(r/r_2)^2} dr.$$

Intuitively, this probability is proportional to the area of the strip between r and $r + dr$, multiplied by the probability that there isn't a closer (within a circle r) vortex. The probability is normalized using the vortex spatial scale, r_2. Finally, we assume that these spatially uncorrelated vortices blink in and out of existence simultaneously over units of time τ. At small scales, the steady flow field of the single, closest vortex will be felt during each time interval. For objects of larger scales, several spatially separated vortices may be felt during each time step.

To account for the variability associated with different realizations of vortex placement, we ensemble average many quantities of interest. For any quantity which is a function of distance to the vortex center, r, we define

$$\langle f(r) \rangle = \int_0^\infty f(r) P(r) dr.$$

Ensemble averaging can be problematic, as no particular oceanic realization will resemble the smoothness of an ensemble average. However, such averaging is necessary to make our problem tractable and we hope that the most salient features are preserved.

4 Short Times / One Vortex

Using this model we can consider what happens to a small dye patch during short times, in which it feels only the effects of a single vortex. The center of mass of the patch will be displaced as a point parcel would be. This displacement is made up of two components, the quick adjustment radial displacement and the slow azimuthal displacement from the equilibrium velocity field. A patch will also be stretched by radial shear, and for long times and high shear could be wrapped up around the vortex center several times. Finally, the patch will be diffusing all this time, both from molecular diffusion and under some circumstances from an enhanced horizontal shear dispersion. Each of these items will be considered in turn below.

4.1 Outward Displacements

The first displacement comes during the adjustment phase and is given by $\zeta(r)$. The ensemble average adjustment displacement felt by a parcel will take into account the probability of being a given distance away from the closest vortex center and is given by

$$\begin{aligned} \langle \zeta(r)^2 \rangle &= \int \zeta^2(r) P(r) dr && (17) \\ &\approx .01 && (18) \end{aligned}$$

where the approximate form was obtained by integrating the numerical $\zeta(r)$ profile shown in Figure 3. As a reminder, these numbers should be scaled by $(h_* N/f)^2$ to return to dimensional units of m^2. Since we don't have a good analytical approximation for $\zeta(r)$ and since it doesn't vary with the main parameter of interest, τ, we aim for just an order of magnitude estimate.

4.2 Azimuthal Displacements

The average azimuthal displacements felt by a parcel moving around a vortex will depend not only on the distance to the vortex center, but also on the length of time τ it has to move. For a given τ and r, the displacement is shown in Figure 4 and is given by

$$\begin{aligned} l^2 &= 2r^2[1 - \cos(\Omega(r)\tau)] \\ \langle l^2 \rangle &= \int_0^\infty P(r) 2r^2 [1 - \cos(\Omega(r)\tau)] dr. && (19) \end{aligned}$$

With $\Omega(r)$ given by 16, it is difficult to solve for $\langle l^2 \rangle$ analytically. However, there are a few limits of interest that are more approachable. For small vortex lifetimes, we can Taylor expand(19) in powers of $(\Omega\tau)$.

$$\langle l^2 \rangle \approx \sum_{n=1}^{\infty} (\Omega_0 \tau)^{2n} \frac{4(-1)^{n-1}}{(2n)!} \int_{r_1}^{\infty} r^3 e^{-(\frac{r}{r_2})^2} e^{2n\alpha(r_1 - r)} dr. \qquad (20)$$

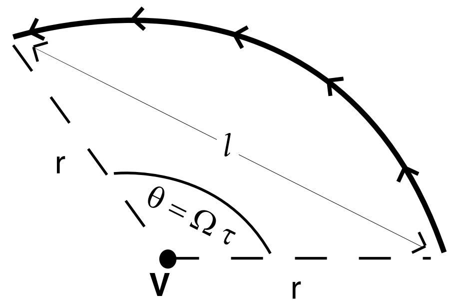

Figure 4: Azimuthal distance traveled during a time τ by a particle a distance r away from the center of the closest vortex (V).

Taking only the first expansion term and integrating gives

$$\langle l^2 \rangle \approx 2(\Omega_0 \tau)^2 e^{-(\frac{r_1}{r_2})^2} \Gamma, \tag{21}$$

where we define

$$\begin{aligned} \Gamma \equiv \; & \frac{r_2^2}{4}[\sqrt{\pi}\alpha r_2 e^{\alpha^2 r_2^2 + 2\alpha r_1 + (r_1/r_2)^2}(3 + 2(\alpha r_2)^2)(\mathrm{erf}(\frac{\mathrm{r_1}}{\mathrm{r_2}} + \alpha \mathrm{r_2}) - 1) \\ & + 2((\frac{r_1}{r_2})^2 - \alpha r_1 + (\alpha r_2)^2 + 1)]. \end{aligned} \tag{22}$$

The upper bound on (19) is obtained by noting that

$$1 - \cos[\Omega(r)\tau] \leq 2,$$

and thus

$$\langle l^2 \rangle \leq \frac{r_2^2}{2}(r_1^2 + r_2^2) e^{-(\frac{r_1}{r_2})^2}. \tag{23}$$

A numerical solution to equation (19) together with the limits given in (21) and (23) is plotted in Figure 5a. The outward displacement magnitude, ζ^2, is also plotted for reference. Figure 5b shows expected squared displacements divided by τ, which is related to the diffusivity expected for a random walk process of given step length. For increasing τ, average displacements approach steady values, but expected diffusivities peak and then decline.

The relative importance of azimuthal versus radial displacements depends on the magnitude of τ. From Figure 5, the two effects achieve equal magnitudes for $\Omega\tau \sim .6$. In coastal areas, we expect outward displacements to be more important, and vice versa for the open ocean. More precisely, the true ensemble average displacement is $\langle (l + \zeta)^2 \rangle$, which is even less analytically tractable. But since

$$\langle l^2 \rangle + \langle \zeta^2 \rangle \leq \langle (l + \zeta)^2 \rangle,$$

calculating them separately gives us an upper bound on average displacement magnitude.

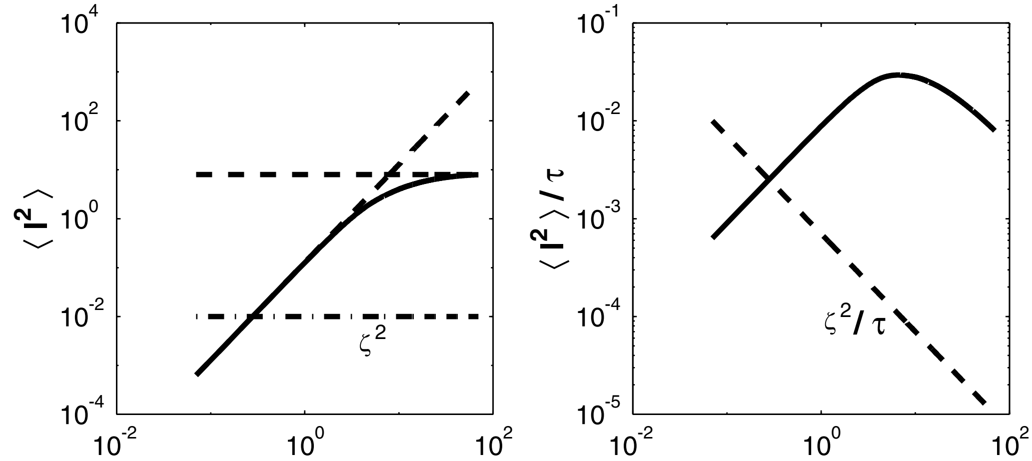

Figure 5: Numerically integrated average squared displacements along with analytically calculated limits are shown in (a). Also shown are adjustment displacements squared for comparison. Random walk diffusivities based on such displacements are shown in (b).

4.3 Azimuthal stretching

While a dye patch moves around a vortex center, it is sheared by radial gradients in velocity. The direction of shear is likely to be different in different periods of time τ. Hence, in calculating stretching we must consider not only the distance to a vortex center but also a dye streak orientation with respect to a vortex. The increase in length of a small line element during one time interval τ is shown in Figure 6 and given by

$$\delta s^2 \equiv \frac{s_1^2}{s_0^2} = [1 + \tau r \frac{d\Omega(r)}{dr} \sin(2\phi) + (\tau r \frac{d\Omega(r)}{dr} \cos\phi)^2].$$

Ensemble averaging must be done over r and ϕ. We assume that ϕ is evenly distributed between 0 and 2π. After N period of length τ have passed, a streak of initial length s_0 will have grown to

$$\begin{aligned} \langle s_N^2 \rangle &= s_0^2 \quad [\langle\langle \delta s(r,\phi)^2 \rangle_\phi \rangle_r]^n \\ &= s_0^2 \quad [\langle 1 + \frac{\tau^2}{2}(r\frac{\delta\Omega(r)}{\delta r})^2 \rangle_r]^n \\ &= s_0^2 \quad e^{-n(r_1/r_2)^2}[1 + \Gamma\alpha^2(\Omega_0\tau)^2]^n. \end{aligned} \tag{24}$$

Equation (24) can be written in a simple exponential form

$$\langle s_N^2 \rangle = e^{2\gamma t}, \tag{25}$$

by defining

$$\gamma \equiv \frac{1}{2\tau}[\ln(1 + \Gamma\alpha^2(\Omega_0\tau)^2) - (\frac{\mathrm{r}_1}{\mathrm{r}_2})^2]. \tag{26}$$

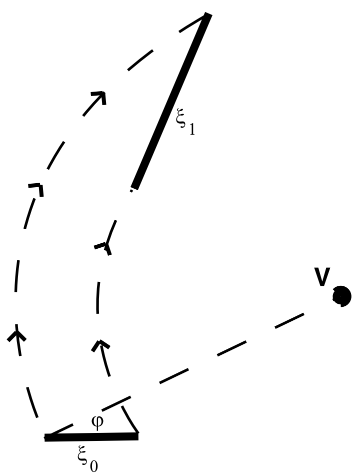

Figure 6: Stretching of a line element.

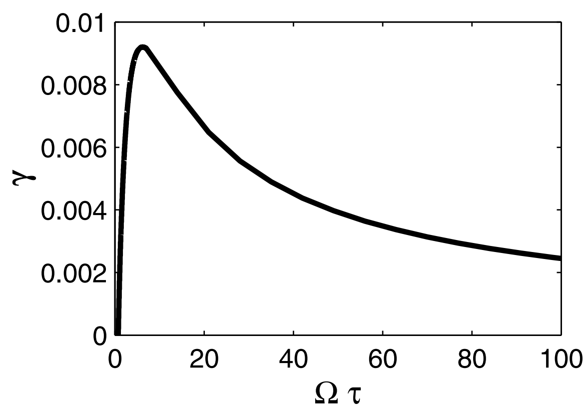

Figure 7: Exponential stretching rate felt over many vortex lifetimes.

One might note the similarity of this to the Lyapunov exponents calculated for the Random Renovating Wave model developed in the principle lectures. The stretching rate, γ, is plotted in Figure 7 as a function of $\Omega\tau$.

4.4 Diffusion/Shear Dispersion

As a dye patch stretches and moves around a vortex center, its area will increase due to horizontal diffusivity. Molecular diffusion in a sheared velocity field is enhanced by the interaction between horizontal or vertical shear and a background horizontal or vertical diffusivity. In a steady shear field, this interaction leads to an anomalously fast diffusion at large times[4]. In an oscillatory flow field, the anomalous diffusion of steady shear is appropriate only for time-scales smaller than the oscillation time. Over several periods, diffusion regains a Fickian character, with an enhanced effective diffusivity which is averaged over the oscillation time of the anomalous diffusion. Young et al. considered the vertical shear associated with typical open ocean values of the internal wave field and found that horizontal diffusion was enhanced over it's molecular values by a factor of N^2/f^2. Our flow similarly contains a finite time scale. In our case, shear is steady for the vortex existence time, τ, after which it may change direction and magnitude. However, unlike the Young et al. model in which the advective solution returns to it's original state at the end of each oscillation, our flow is circular within each time period. Therefore, Rhines and Young's work on two-dimensional dispersion for closed streamlines is also helpful[11]. The shear in their case is radial shear of a circular flow. To get the best shear dispersion estimate for our problem, we start with the Rhines and Young approach and add a vertical component of shear and time dependence.

Following their approach, we start with the advection diffusion equation for concentration, θ in a steady velocity field. For a circular velocity field with azimuthal velocity given by

$$\frac{1}{r}u_\phi = \Omega(r,z) \tag{27}$$

and distinct vertical and horizontal diffusivities, the governing equation is

$$\theta_t + \Omega\theta_\phi = K_H[\frac{1}{r}(r\theta_r)_r + \frac{1}{r^2}\theta_{\phi\phi}] + K_z\theta_{zz} \tag{28}$$

If we assume that there is an independent internal wave field with a faster time scale superimposed on our vortical mode field, a plausible relationship between K_H and K_z is given by [4]

$$K_H = \frac{N^2}{f^2}K_z. \tag{29}$$

We assume the solution can be written as a sum of components with different azimuthal wavenumbers, each of which is given by

$$\begin{aligned} \theta &= A(r,z,t)e^{in\hat{\phi}} && (30)\\ \hat{\phi} &\equiv \phi - \Omega(r,z)t. && (31) \end{aligned}$$

Plugging (30) into (28) and grouping terms gives an equation for the rate of concentration change in the framework of the advective solution

$$\begin{aligned} A_t \;=\; & K_H[\frac{1}{r}(rA_r)_r + \frac{n^2}{r^2}A] + K_zA_{zz} \\ & -i\{K_H[\frac{A}{r}(r\bar{\Omega}_r)_r + 2A_r\bar{\Omega}_r] + K_z[A\bar{\Omega}_{zz} + 2A_z\bar{\Omega}_z]\} \\ & -\{K_HA\bar{\Omega}_r^2 + K_z\bar{\Omega}_z^2)\}, \end{aligned} \tag{32}$$

with

$$\bar{\Omega} \equiv nt\Omega.$$

The rhs terms of (32) are grouped by powers of $(nt\Omega)$, which is physically related to distance traveled around the vortex center. Analysis in section 2 indicated that oceanic vortical modes can have existence times that vary from much shorter to much longer than

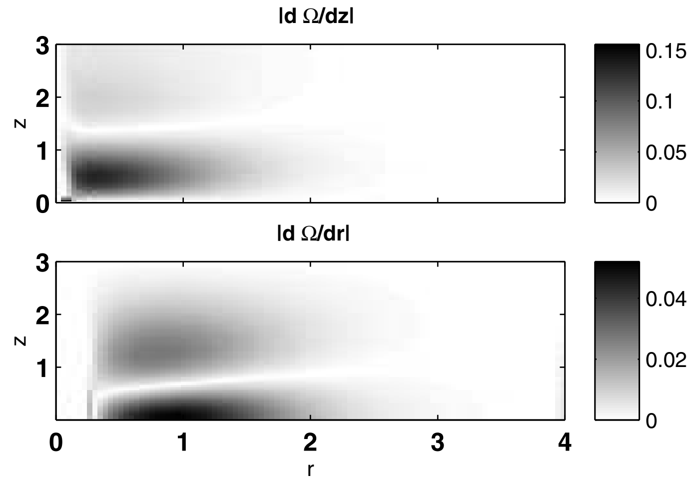

Figure 8: Non-dimensional magnitude of vertical and horizontal shear from the full numerical solutions for an equilibrium vortex velocity field.

their eddy turnover time such that we are interested in solutions for a range of $\bar{\Omega}$ values. The first term in (32) is simply molecular diffusion, and in the limit of $\bar{\Omega} \ll 1$, this is the dominant term. In the opposite limit, $\bar{\Omega} \gg 1$, the third term of (32) dominates. This is the limit considered by Rhines and Young. Following their analysis, the solution to (32) for large $\bar{\Omega}$ becomes

$$A \sim e^{-\frac{1}{3}n^2 t^3 [K_H \Omega_r^2 + K_z \Omega_z^2]}. \tag{33}$$

For intermediate values of $\bar{\Omega}$, we need to use the full version of (32). Such precision is beyond the scope of this paper, and unnecessary to get the sort of magnitude estimates we are interested in. The above approximations suggest that for vortices with short lifetimes (coastal regions), vortical shear dispersion is not significant, and we can define an appropriate effective horizontal diffusivity, K_s which is in this case equal to the traditionally used internal wave enhanced value given by (29). In areas with long lived vortices (open ocean), this traditional value is likely to be further enhanced by vortical mode shear dispersion. Roughly following methods of dealing with oscillatory waves in Rhines and Young and Young et al., we pull from (33) an effective diffusivity of the form

$$K_s \sim \frac{1}{6} n^2 \tau^2 \langle K_H \Omega_r^2 + K_z \Omega_z^2 \rangle. \tag{34}$$

K_H is given by (29) and K_z is perhaps a molecular diffusivity. Radial and vertical shears from the McWilliams model are shown in Figure 8. The reader will recall that these shears are non-dimensional and dimensional forms of Ω_r^2 and Ω_z^2 will have a relative scaling factor of N^2/f^2. Hence, the roughly comparable magnitudes shown in Figure 8 indicate comparable importance of the two terms in (34).

All of the abovementioned effects (stretching, shear dispersion, net displacement) occur at the same time for a dye patch feeling a single vortex field. To gain some insight into how

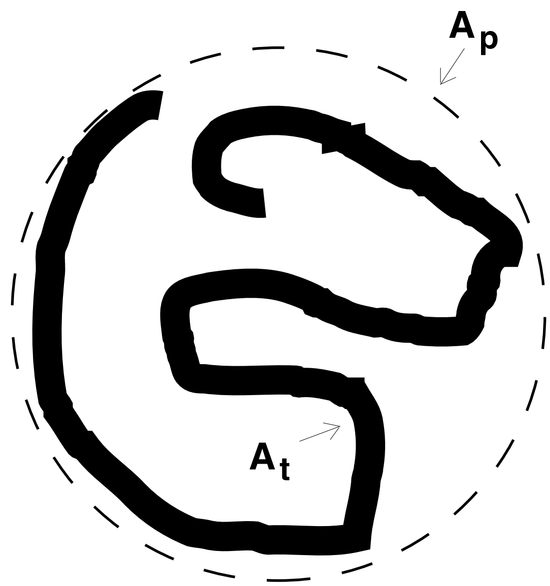

Figure 9: Schematic of different growth rates that characterize tracer distribution.

these various effects fit together into a more coherent picture of diffusion, we now turn to longer time scales.

5 Longer Times

During longer time periods, a dye patch will experience the effects of multiple vortices, both because we are considering times greater than an individual vortex lifetime and because over long times a patch grows spatially to feel many vortices. As a dye patch is stretched by several randomly oriented vortices in turn, it stretches and folds as illustrated in the cartoon in Figure 9. There are now two types of diffusion of interest. First, one might like to know the size of the bounding circle, designated as A_p in Figure 9. This represents the area in which one has a chance of encountering concentrate. As suggested by Garrett, this area grows as the separation between discrete parcels in the flow field[3]. The second quantity of interest is the actual area occupied by dye, A_t, which will depend on the stretching rate γ from equation (26). We now approach both these quantities more specifically for our RRV flow field.

5.1 Multiparticle Dispersion

The bounding area, A_p, will roughly grow like the size of a group of discrete water parcels initially close together. Qualitatively, the dispersion rate of a collection of particles is a function of how close they are to each other. A group of closeby particles will all be feeling a similar velocity field and will move more or less together, dispersed only by the small velocity differences between their positions. As they move apart, they feel a larger velocity difference and move apart more quickly. In our case there comes a point when they are so far separated that (on average) they no longer feel the same vortex, at which point their velocities become completely uncorrelated. At this point each particle moves in its own random walk and the particle separation distance should increase as twice that of a single random walker.

Quantitatively, the area of a group of particles is described by the second moment,

$$\sigma^2 \equiv \frac{1}{n}\sum_{i=1}^{n}(x_i-\bar{x})^2 = \frac{1}{n}\sum_{i=1}^{n}x_i^2 - \bar{x}^2, \tag{35}$$

with

$$\bar{x} \equiv \frac{1}{n}\sum_{i=1}^{n}x_i.$$

Parcel position x_i at any time t can be obtained by integrating the Lagrangian velocity field

$$x_i \equiv x_{i0} + \int_0^t u_i(t')dt'. \tag{36}$$

Plugging (36) into (35) gives

$$\begin{aligned}\sigma^2 &= \sigma_0^2 + \frac{1}{n}\sum_{i=1}^{n}\left[\int_0^t u_i(t')dt'\right]^2 \\ &\quad -\frac{1}{n^2}\sum_{i=1}^{n}\sum_{j=1}^{n}\int_0^t u_i(t')dt'\int_0^t u_j(t'')dt''. \end{aligned}\tag{37}$$

For our model, $t = N\tau$, where N is the number of vortex lifetimes experienced. The net displacement, $x_i(t)$, is simply the sum of displacement from each successive vortex

$$\int_0^t u_i(t')dt' = \sum_{k=1}^{N}\int_0^\tau u_i^{(k)}(t')dt'.$$

Next, we simplify by ensemble averaging (37). Consider how variance increases on average during one period

$$\begin{aligned}\langle\sigma_N^2\rangle - \langle\sigma_{N-1}^2\rangle &= \langle\frac{1}{n}\sum_{i=1}^{n}\left[\int_0^\tau u_i(t')dt'\right]^2\rangle \\ &\quad -\langle\frac{1}{n^2}\sum_{i=1}^{n}\sum_{j=1}^{n}\int_0^\tau u_i(t')dt'\int_0^\tau u_j(t'')dt''\rangle,\end{aligned}$$

which can be re-written as

$$\begin{aligned} &= \frac{1}{n}\sum_{i=1}^{n}\langle l^2\rangle - \frac{1}{n^2}\sum_{i=1}^{n}\sum_{j=1}^{n}\langle l_i l_j\rangle \\ &= \frac{1}{n}\sum_{i=1}^{n}\langle l^2\rangle[1-\frac{1}{n}\sum_{j=1}^{n}\frac{\langle l_i l_j\rangle}{\langle l^2\rangle}]. \end{aligned}\tag{38}$$

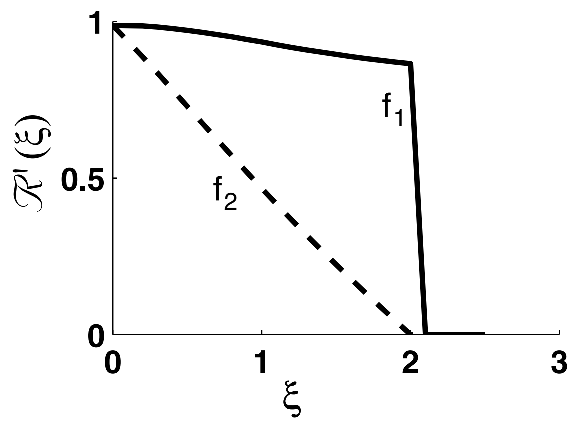

Figure 10: Two different possibilities for multiparticle spatial correlation.

Here $\langle l^2\rangle$, from (19) is the same for each parcel and $\langle l_i l_j\rangle$ is a measure of correlation between a pair of parcels and must be summed over all pair combinations. Physically, (38) states that the increase in particle area goes like the single particle diffusivity with a correction term that accounts for correlation between particles. If all particles are moving with the same, perfectly correlated velocity, $\langle l_i l_j\rangle = \langle l^2\rangle$, then no relative dispersion occurs. In our flow, the degree of correlation is a function of the particle separation, $\langle l_i l_j\rangle = \mathcal{F}[\langle \sigma^2_{N-1}\rangle]$.

To make this calculation more tractable, consider the evolution of distance between only two particles. Let $\langle \xi^2\rangle = \mathbf{x_2} - \mathbf{x_1}$ be the distance between two parcels. The ensemble averaged increase in $\langle \xi^2\rangle$ during any single time period is given by

$$\langle \xi^2_N\rangle - \langle \xi^2_{N-1}\rangle = 2\langle l^2\rangle[1 - \frac{\langle l^2_{ij}(\xi_{N-1})\rangle}{\langle l^2\rangle}] \tag{39}$$

For two parcels a distance ξ apart, $\langle l_i l_j\rangle$ is given by

$$\langle l^2_{ij}\rangle = \int_0^\infty \int_0^{2\pi} P(r)2r(r+\delta r)\sqrt{[1-\cos(\Omega(r)\tau)][1-\cos(\Omega(r+\delta r)\tau)]}d\phi dr, \tag{40}$$

with

$$\delta r \equiv \sqrt{\frac{\xi^2}{4} + r^2} - \sqrt{\frac{\xi^2}{4} - \xi r\cos(\phi) + r^2}.$$

We define a spatial correlation function

$$\mathcal{R}_{ij} \equiv \frac{\langle l_i l_j\rangle}{\langle l^2\rangle}. \tag{41}$$

As is, this representation assumes that as particles grow further apart their velocity becomes less correlated but they still feel different parts of the same vortex field. It is more realistic to say that significantly separated particles will feel the effects of uncorrelated vortices. From

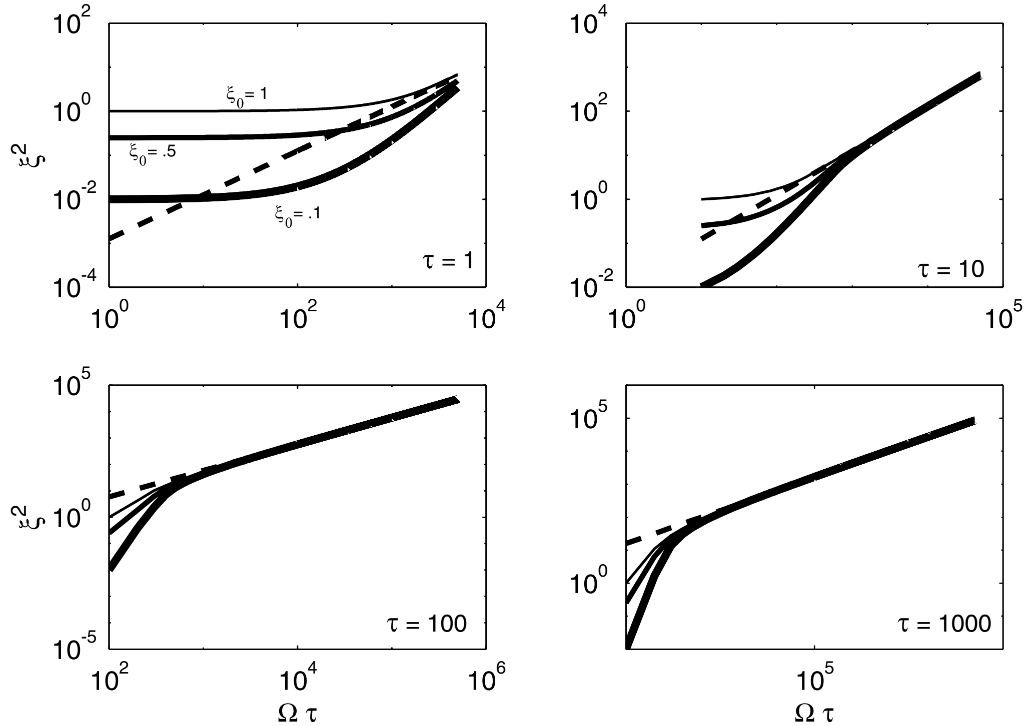

Figure 11: Squared pair separation distance obtained by iterative integration. τ ranges from 1 to 1000. In all subplots the solid lines represent ξ_0 values of .1,.5 and 1. The dotted line is the growth rate expected for uncorrelated randomly walking particles.

Section 2, the lengthscale of vortex influence is r_2. We manually impose this constraint by defining a new correlation function in which particles greater than r_2 away feel different vortices

$$\mathcal{R}'(\xi) \equiv (\mathcal{R})(\xi) f(\xi), \tag{42}$$

where $f(\xi)$ is some function that goes from 1 at $r = 0$ to 0 for large r. There are several forms $f(\xi)$ can take. We could impose that correlation abruptly goes to 0 when the distance exceeds r_2, so $f(\xi)$ takes the form of a Heavyside step function

$$f_1(\xi) = \begin{cases} 1 & r < r_2 \\ 0 & r \geq r_2. \end{cases} \tag{43}$$

This is straightforward but a little abrupt. Another possibility is to make the transition very smooth by assuming that the probability of nearby particles being in different vortices goes from 0 to 1 linearly:

$$f_2(\xi) = 1 - \frac{\xi}{R_0}. \tag{44}$$

Both possibilities for $\mathcal{R}'$ are plotted in Figure 10, where R_{ij} has been numerically calculated from (19) and (40) for different values of ξ. Reality is likely to be somewhere in between. The second choice has the advantage of a continuous derivative. It also provides an approximate lower bound for parcel spatial correlation and hence an upper bound for diffusion rate. We will use the form in (44) from now on.

The real quantity of interest is the time evolution of ξ for particles initially separated by a distance ξ_0. We numerically integrate (39) for different values of ξ_0 and τ and plot the results in Figure 11. For reference, we also plot the separation growth expected for uncorrelated particles based on (19) alone, assuming $\langle l_i l_j \rangle = 0$. At large times, particle separation goes as twice the single particle dispersion rate, $\langle l^2 \rangle$, as expected. For a given value of τ, the initial particle separation, ξ_0, controls the time it takes to settle into linear growth, but not the qualitative nature of the transition or any aspect of the large time solution. For different values of τ, several things change. First, the final diffusivity (the intercept of our log-log plot) is different, as expected from the relationship in Figure 5. Second, the transition to linear growth has a different character. For $\tau = 1, 10$, the initial growth in $\langle \xi^2 \rangle$ is slower than linear, while for $\tau = 100, 1000$ it grows with a faster than linear growth rate.

5.2 Streak Area

The other way to characterize the growth of a dye streak is by the actual area of the tracer. As described by Ledwell et al. and Sundermeyer, the streak will go through an initial period of stretching during which it gets thinner, cross-streak gradients get larger and cross-streak diffusive fluxes grow. Eventually a balance between stretching and diffusion is reached, at which point the streak continues to grow larger, but its width remains the same. This equilibrium width is related to the stretching rate γ (26), by

$$\Delta l = \sqrt{\frac{K_s}{\gamma}} \tag{45}$$

where K_s is an appropriate horizontal diffusivity (section 4.4).

After a width is established, the streak area grows with its increasing length

$$\begin{aligned} A_t &= (\Delta l)(l) \\ &\sim l_0 \sqrt{\frac{K_s}{\gamma}} e^{\gamma t} \end{aligned} \tag{46}$$

for some initial length l_0.

5.3 The Big Picture

During the initial period of stretching and folding of a dye patch, the containing area A_p will be significantly larger than the actual dye area A_t. However, tracer area grows exponentially, (46), and will catch up. Physically, as the tracer area depicted in Figure 9 grows, different parts of the tracer streak get close enough together that they start to merge and the tracer fills in the area bounded by A_p. From then on, the dye patch is fairly homogeneous, and continues to grow in a Fickian manner with A_p. In Figure 12, we plot $A_p(t)$ and $A_t(t)$ together

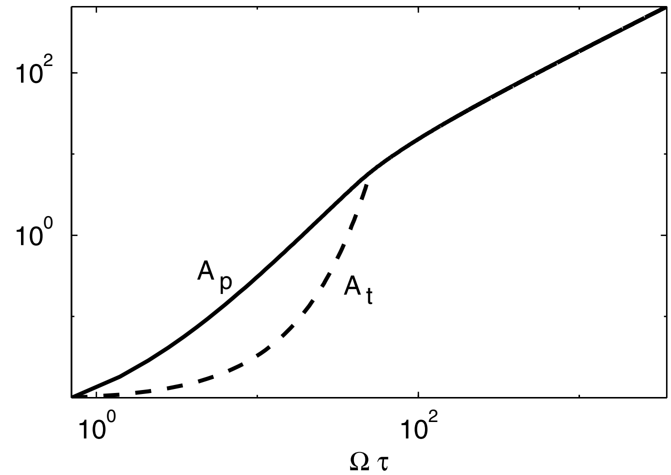

Figure 12: Growth rates for multiparticle dispersion and tracer area. They merge

for $\gamma = .008, \tau = 100, \xi_0 = .1$. We have assumed that both quantities start with the same initial area,

$$A_0 \equiv l_0 \sqrt{\frac{K_s}{\gamma}} = \xi_0^2.$$

In this case, tracer area is much smaller than the bounding area up until a time $\Omega\tau_0 \sim 70$, after which tracer area grows linearly as A_p.

6 Ocean comparisons and Conclusions

Our goal in this work has been to evaluate whether sub-mesoscale eddies could make a significant contribution to horizontal diffusion in the coastal or open ocean. Because it was not immediately apparent which of the potential stirring and mixing abilities of vortical modes would be important, we undertook a step by step look at the time dependent diffusion of an initially small patch of passive tracer. To get a realistic form for a single vortical mode, we looked at numerical solutions to the non-linear adjustment of an isolated density anomaly, and incorporated an idealized version of these results into a simple stochastic renovating vortex model. Most of the qualitative features of qualitative tracer evolution we discuss are the same as those described by Garrett for a two-dimensional turbulent field. Using our analytical model, we're able to calculate exact values for some of the stages he talks about more qualitatively. The picture that emerges is that at space and time scales of the same order of magnitude of vortex scales and lifetimes, a patch of dye twists and folds with exponentially increasing area, filling a larger bounding area governed by the multiparticle dispersion rate. At larger space and time scales, the tracer area grows in a fickian manner with the effect of vortical modes incorporated into an effective diffusivity.

In a realistic ocean, the added complexities of stirring processes operating on a variety of time and space scales will prohibit comparison of the distinct stages of diffusion we've discussed. The most practical results to emerge from our work are estimates of an effective (Fickian) diffusvity, and bounds on when such a diffusivity is appropriate. In the coastal ocean, vortex lifetimes are likely to be shorter than their turnover timescale. In this limit, the displacements, stretching distortion and shear dispersion associated with azimuthal motion may not be as important as displacements from the initial vortex adjustment. We calculate a non-dimensional effective diffusivity for this random-walk like motion of .01 (Figure 5.) To redimensionalize, we multiply by $(N^2 h_*^2 f\beta)/f^2$. Using $N = 10$ cph, $f = 1$ day^{-1}, $\beta = .25$, and $h_* =$ 3-10 m, we get dimensional diffusivities of up to .1 m^2/s. While this is an enhancement over the estimates from shear dispersion alone, it is still an order of magnitude smaller than observations. In the open ocean, vortices may exist for many rotations, in which case the mechanisms of Section 5 are more appropriate. Using h_* up to 30 m, we calculate dimensional diffusivities of order 1 m^2/s, the same order as observations. This value will be appropriate only after a dye patch has grown to scales larger than the vortex scale (approximately an internal Rossby radius). Our analysis suggests the time necessary to get there is highly dependent on the initial dye patch size and the vortex lifetime (Figure 11).

There are numerous additional complexities that could be included in future work. First, given the importance of the vortex lifetime, τ in our results, we should try to get better estimates of realistic ocean values. We should consider the potential effect of instabilities as a limit on expected lifetime. Second, we could consider a model with a continuous distribution of vortex lifetimes. Third, we could use a the full baroclinic vortex form suggested by the numerical adjustment results. Such an approach would include the effects of cyclonically rotating vortices, which could significantly enhance stirring motions. Finally, we could compare our analytical results with full numerical simulations, such as those being performed by P. Lelong [12].

7 Acknowledgements

I'd like to thank Jim Ledwell and Miles Sundermeyer for suggesting this project and being patient and helpful throughout. I also thank Bill Young, Glenn Flierl, Antonello Provenzale, Claudia Pasquero, Jean-Luc Thiffeault, and Stefan Llewellyn Smith for numerous helpful discussions. I'm indebted to Neil Balmforth, Bill Young and the entire GFD staff for giving me the opportunity to participate in the summer program and for all the wisdom they generously share. The summer was infinitely enhanced by the company of the other fellows for lively (and only occasionally squalid) dinners, triathalons, beach trips, and softball games. Thanks especially to Nifer, Claudia and J-Luc for their friendship and support.

References

[1] M. A. Sundermeyer, Ph.D. thesis, WHOI, 1998.

[2] J. Ledwell, A.J.Watson, and C. Law, "Evidence for slow mixing across the pycnocline from an open-ocean tracer-release experiment," Nature **364**, 701 (1993).

[3] C. Garrett, “On the initial streakiness of a dispersing tracer in two- and three-simensional turbulence,” Dyn. Atmos. Oceans 265 (7).

[4] W. Young, P. Rhines, and C. Garrett, “Shear-flow dispersion, internal waves and horizontal mixing in the ocean,” J. Phys. Ocean. **12**, 515 (1982).

[5] J. McWilliams, “Submesoscale, coherent vortices in the ocean,” Rev. Geophys. **23**, 165 (1985).

[6] K. Polzin, E. Kunze, J. Toole, and R. Schmitt, in progress (unpublished).

[7] M.C.Gregg, E. D’Asaro, T. Shay, and N. Larson, “Observations of persistent mixing and near-inertial internal waves,” J. Phys. Ocean. **16**, 856 (1986).

[8] N. Oakey, personal communication.

[9] J. McWilliams, “Vortex generation through balanced adjustment,” J. Phys. Ocean. **18**, 1178 (1988).

[10] W. Blumen, “Geostrophic adjustment,” Rev. Geophys. and Space Phys. **10**, 485 (1972).

[11] P. Rhines and W. Young, “How rapidly is a passive scalar mixed within closed streamlines?,” J. Fluid Mech. **133**, 133 (1983).

[12] P. Lelong, personal communication.